

# Ising ferromagnets and antiferromagnets in an imaginary magnetic field

Roman Krčmár, Andrej Gendiar and Ladislav Šamaj

*Institute of Physics, Slovak Academy of Sciences, Dúbravská cesta 9, 84511 Bratislava, Slovakia*

(Dated: March 31, 2022)

We study classical Ising spin- $\frac{1}{2}$  models on the 2D square lattice with ferromagnetic or antiferromagnetic nearest-neighbor interactions, under the effect of a pure imaginary magnetic field. The complex Boltzmann weights of spin configurations cannot be interpreted as a probability distribution which prevents from application of standard statistical algorithms. In this work, the mapping of the Ising spin models under consideration onto symmetric vertex models leads to real (positive or negative) Boltzmann weights. This enables us to apply accurate numerical methods based on the renormalization of the density matrix, namely the corner transfer matrix renormalization group and the higher-order tensor renormalization group. For the 2D antiferromagnet, varying the imaginary magnetic field we calculate with a high accuracy the curve of critical points related to the symmetry breaking of magnetizations on the interwoven sublattices. The critical exponent  $\beta$  and the anomaly number  $c$  are shown to be constant along the critical line, equal to their values  $\beta = \frac{1}{8}$  and  $c = \frac{1}{2}$  for the 2D Ising in a zero magnetic field. The 2D ferromagnets behave in analogy with their 1D counterparts defined on a chain of sites, namely there exists a transient temperature which splits the temperature range into its high-temperature and low-temperature parts. The free energy and the magnetization are well defined in the high-temperature region. In the low-temperature region, the free energy exhibits singularities at the Yang-Lee zeros of the partition function and the magnetization is also ill-defined: it varies chaotically with the size of the system. The transient temperature is determined as a function of the imaginary magnetic field by using the fact that from the high-temperature side both the first derivative of the free energy with respect to the temperature and the magnetization diverge at this temperature.

PACS numbers: 05.50.+q, 64.60.Cn, 64.60.Fr, 64.60.ae, 68.35.Rh, 75.10.Hk

## I. INTRODUCTION

Simulations of many systems in high-energy physics (QCD at finite baryon density) and condensed matter (Hubbard model, antiferromagnetic quantum spin chains, etc.) suffer from a severe sign problem. For such systems, the complex Boltzmann weights of microscopic configurations cannot be interpreted as a probability distribution which prevents from application of standard statistical algorithms.

A prototype of systems with a severe sign problem in equilibrium statistical mechanics is the Ising model of classical spins- $\frac{1}{2}$  on a lattice with nearest-neighbor ferromagnetic or antiferromagnetic interactions, under the effect of a pure imaginary magnetic field. Similar generalizations in quantum mechanics are related to non-Hermitian deformations of the transverse Ising quantum chains, e.g., via the inclusion of an imaginary longitudinal field [1–3]. The Ising model in an imaginary field was investigated mainly in its antiferromagnetic version, on two-dimensional (2D) square or honeycomb lattices. The first studies were oriented to the location of Yang-Lee zeros of the partition function in the complex magnetic field plane and Fisher zeros in the complex temperature plane [4–7]. Similarly as in the case of the real magnetic field [8–10], dividing the lattice into two interwoven sublattices  $A$  and  $B$  the antiferromagnet exhibits two possible phases: the disordered paramagnetic phase at high temperatures with equivalent sublattice magnetizations  $m_A = m_B$  and the symmetry-broken antiferromagnetic phase at low temperatures with  $m_A \neq m_B$ . As the imag-

inary magnetic field varies, the two phases are separated by a curve of critical points. This curve was specified with a good accuracy by computing the first eight cumulants of the high-temperature expansion of the free energy in Ref. [11]. The mean-field analysis of the Ising antiferromagnet in an imaginary magnetic field on a  $D$ -dimensional hypercubic lattice was carried out in [12].

The Ising antiferromagnet in an imaginary magnetic field is exactly solvable in one dimension (1D), see e.g. [12, 13], where second-order phase transitions are absent. As concerns 2D, the exact solution of the antiferromagnetic Ising model is known for zero field [14] and for the (dimensionless) field  $i\pi/2$  [15].

The exact and numerical results obtained so far are restricted mainly to the antiferromagnetic regime in 1D and 2D. The ferromagnetic version of the model is not properly defined since it does not correspond to a unitary theory for any value of the ferromagnetic coupling [15, 16]. Consequently, the free energy and the magnetization per site of the ferromagnet are not defined in the low-temperature region below certain transient temperature [16]. Both in 1D and 2D, there exists a first-order phase transition from the thermodynamically well-behaved high-temperature region to the ill-defined low-temperature region at the transient temperature. As is shown in this paper, the transient temperature can be detected from the high-temperature side as either the divergence of the first derivative of the free energy with respect to the coupling constant or the divergence of the magnetization.

The aim of the present paper is twofold. Firstly, for an

arbitrary  $D$ -dimensional lattice, we construct a mapping of the antiferromagnetic and ferromagnetic Ising models in an imaginary field onto a symmetric vertex model whose local vertex (Boltzmann) weights are real (positive or negative) numbers. Secondly, the vertex representation of the original spin model permits us to apply standard statistical methods, in particular accurate numerical techniques based on the idea of renormalization group applied to the density matrix. For 2D antiferromagnets, varying the imaginary magnetic field we calculate with a high accuracy the curve of critical points and show the uniformity of the critical exponent  $\beta$  and the anomaly number  $c$  along this curve. As concerns 2D ferromagnets, the transient temperature below which the free energy and the magnetization are not defined is determined as a function of the imaginary magnetic field by using two different approaches.

The paper is organized as follows. In Sec. II, we recapitulate briefly the 1D exactly solvable case and discuss anomalies in the ferromagnetic version of the Ising model in an imaginary field. Sec. III deals with the mapping of the partition function of the Ising model in an imaginary field onto the one of a symmetric vertex model on the same lattice structure which exhibits real (positive or negative) local Boltzmann vertex weights. The mapping is constructed for both antiferromagnetic and ferromagnetic cases. Applied numerical methods are described briefly in Sec. IV; some technicalities are moved to Appendix. Numerical results for the critical properties of the 2D Ising antiferromagnets are presented in Sec. V. Numerical results for the 2D Ising ferromagnets are summarized in Sec. VI. The emphasis is put on phenomena close to the first-order transition temperature from the high-temperature to the low-temperature regimes. Sec. VII is a résumé of the obtained results with concluding remarks.

## II. RECAPITULATION OF THE 1D CASE

The 1D chain of  $N$  Ising spins  $\{s_j = \pm 1\}_{j=1}^N$  with nearest-neighbor couplings  $J$  in a magnetic field  $h$  is defined by the Hamiltonian

$$H = -J \sum_{j=1}^N s_j s_{j+1} - h \sum_{j=1}^N s_j, \quad (1)$$

with the cyclic boundary condition  $s_{N+1} \equiv s_1$ . The partition function is given by

$$Z_N = \sum_{\{s\}} e^{-\beta H}, \quad (2)$$

where  $\beta = 1/(k_B T)$  is the inverse temperature and the summation goes over all  $2^N$  spin configurations. Let us denote  $\beta J \equiv F$  and consider the pure imaginary magnetic field  $\beta h \equiv i\theta/2$ . Shifting  $\theta$  by  $2\pi$  induces for each vertex the same factor  $e^{\pm i\pi} = -1$  which has no relevant effect on the partition function (2). The partition

function is also invariant with respect to the transformation  $\theta \rightarrow -\theta$  and therefore one can restrict oneself to  $\theta \in [0, \pi]$ . The  $2 \times 2$  transfer matrix

$$T = \begin{pmatrix} e^{F+i\frac{\theta}{2}} & e^{-F} \\ e^{-F} & e^{F-i\frac{\theta}{2}} \end{pmatrix} \quad (3)$$

has two eigenvalues of the form

$$\lambda_{\pm}(\theta) = e^F \cos\left(\frac{\theta}{2}\right) \pm \sqrt{e^{-2F} - e^{2F} \sin^2\left(\frac{\theta}{2}\right)}. \quad (4)$$

The partition function (2) is determined by the eigenvalues of the transfer matrix as follows

$$Z_N = \lambda_+^N + \lambda_-^N. \quad (5)$$

The free energy per spin  $f$  is defined by

$$-\beta f_N = \frac{1}{N} \ln Z_N \quad (6)$$

and the magnetization per spin  $m_N = \langle s_j \rangle$ , which in 1D does not depend on the site index  $j = 1, 2, \dots$ , by

$$m_N = -\frac{\partial}{\partial \beta h} \beta f_N = 2i \frac{\partial}{\partial \theta} \beta f_N. \quad (7)$$

Note that the magnetization  $m_N$ , which is bounded by  $0 < |m| \leq 1$  for real magnetic fields, can have magnitude larger than 1 for imaginary magnetic fields.

The spin system is usually studied in the thermodynamic limit  $N \rightarrow \infty$ . The analysis of the above equations depends on whether the (dimensionless) coupling constant  $F$  is positive (ferromagnet) or negative (antiferromagnet).

### A. 1D antiferromagnet

If  $F < 0$ , the argument of the square root in (4) is always positive which implies real eigenvalues  $\lambda_{\pm}$ ,  $\lambda_+ > 0$  and  $\lambda_- < 0$ ; since  $\lambda_+ > |\lambda_-|$  the partition function (5) is real and positive. In the limit  $N \rightarrow \infty$ , from the two summands in (5)  $\lambda_+^N$  dominates, so that the free energy per site  $f = \lim_{N \rightarrow \infty} f_N$  is given by

$$-\beta f = F + \ln \left[ \cos\left(\frac{\theta}{2}\right) + \sqrt{e^{-4F} - \sin^2\left(\frac{\theta}{2}\right)} \right]. \quad (8)$$

The magnetization per site  $m = \lim_{N \rightarrow \infty} m_N$  is given by

$$-im = \frac{\sin\left(\frac{\theta}{2}\right)}{\sqrt{e^{-4F} - \sin^2\left(\frac{\theta}{2}\right)}}. \quad (9)$$

There is no second-order phase transition in 1D.

## B. 1D ferromagnet

If  $F > 0$ , the argument of the square root in (4) can have both positive and negative signs. For a fixed value of  $\theta \in [0, \pi]$ , let us introduce a “transition” coupling  $F^*(\theta)$ ,

$$e^{-2F^*} = \sin\left(\frac{\theta}{2}\right), \quad (10)$$

at which the argument of the square root in (4) vanishes.

In the high-temperature region  $0 < F < F^*$ , the argument of the square root is positive which implies that  $\lambda_+ > |\lambda_-|$  and one can use the previous formulas (8) and (9). Note that as  $F$  approaches  $F^*$  the magnetization (9) diverges.

In the low-temperature region  $F > F^*$ , the argument of the square root is negative and, consequently, the complex conjugate eigenvalues

$$\lambda_{\pm}(\theta) = e^F \cos\left(\frac{\theta}{2}\right) \pm i\sqrt{e^{2F} \sin^2\left(\frac{\theta}{2}\right) - e^{-2F}} \quad (11)$$

have in polar coordinates the same modulus and the opposite phases:

$$\lambda_{\pm}(\theta) = \sqrt{e^{2F} - e^{-2F}} \exp(\pm i\varphi), \quad (12)$$

where

$$\varphi(F, \theta) = \arccos\left[\frac{\cos\left(\frac{\theta}{2}\right)}{\sqrt{1 - e^{-4F}}}\right]. \quad (13)$$

The partition function (5) reads as

$$Z_N = 2(e^{2F} - e^{-2F})^{N/2} \cos(N\varphi), \quad (14)$$

The Yang-Lee zeros of the partition function thus exist exclusively in the low-temperature region  $F > F^*$  and correspond to the following irrational values of  $\varphi$ :

$$\varphi(F, \theta) = \frac{2j-1}{2N}\pi, \quad j = 1, 2, \dots, N. \quad (15)$$

Since  $Z_N = 0$ , the free energy goes to  $-\infty$  at these points which become dense in the limit  $N \rightarrow \infty$ . This means that the free energy is not defined for  $F > F^*$ .

As is shown in this paragraph, it is a mathematical curiosity that if one fixes the value of  $\varphi$  outside of the Yang-Lee set (15), say  $\varphi$  is a rational number, the expression for the free energy converges when increasing the number of sites  $N \rightarrow \infty$ . The term  $\cos(\varphi N)$  will change its sign with increasing  $N$ . The oscillating sign of the partition function does not represent any problem in the definition of the free energy per spin (6) since the principal value of the complex logarithm  $\ln(-1) = i\pi$ , when divided by  $N$ , goes to 0 in the limit  $N \rightarrow \infty$ . Taking the absolute value of the partition function in the definition of the free energy per spin (6), one gets

$$-\beta f_N = \frac{1}{2} \ln(e^{2F} - e^{-2F}) + \frac{1}{N} \ln|2 \cos(N\varphi)|. \quad (16)$$

Using the formula [17]

$$2 \cos(N\varphi) = 2^N \prod_{k=1}^N \sin\left(\varphi + \frac{2k-1}{2N}\pi\right), \quad (17)$$

one obtains that

$$\frac{1}{N} \ln|2 \cos(N\varphi)| = \ln 2 + \frac{1}{N} \sum_{k=1}^N \ln \left| \sin\left(\varphi + \frac{2k-1}{2N}\pi\right) \right|. \quad (18)$$

According to the Euler-Maclaurin formula [18]

$$\begin{aligned} \sum_{n=a}^b f(n) &\sim \int_a^b dx f(x) + \frac{1}{2} [f(a) + f(b)] \\ &+ \sum_{k=1}^{\infty} \frac{B_{2k}}{(2k)!} [f^{(2k-1)}(b) - f^{(2k-1)}(a)] \end{aligned} \quad (19)$$

with  $a, b$  being integers and  $\{B_{2k}\}$  the Bernoulli numbers, the discrete sum on the rhs of (18) is nothing but a Riemann integral plus large- $N$  corrections. The set of Yang-Lee zeros (15) becomes dense in the thermodynamic limit  $N \rightarrow \infty$ . If  $\varphi$  belongs to the set of Yang-Lee zeros (15), the continualization of (18) is not possible as one of the summands, namely the one with  $j+k-1=N$ , diverges. When  $\varphi$  does not belong to the set of Yang-Lee zeros (15), say it is a rational number at an infinitesimal distance  $1/N$  from Yang-Lee zeros in its neighborhood, the problematic summand in (18) is of order  $\ln[\sin(1/N)]/N \sim -(\ln N)/N$  and vanishes in the limit  $N \rightarrow \infty$ , so that

$$\frac{1}{N} \ln|2 \cos(N\varphi)| = \ln 2 + \int_0^1 dt \ln|\sin(\varphi + \pi t)| + o(1). \quad (20)$$

The integral over  $t$  exactly cancels the term  $\ln 2$  for any value of  $\varphi$ . We then suggest that as soon as  $\varphi$  is a rational number, the thermodynamic  $N \rightarrow \infty$  limit of the lhs of Eq. (20) exists and equals to 0; one can check this suggestion numerically by fixing  $\varphi$  (say to an integer) and going with  $N$  to extremely large values. The thermodynamic limit of the free energy then reads as

$$-\beta f = \frac{1}{2} \ln(e^{2F} - e^{-2F}). \quad (21)$$

Thus, excluding from the consideration the set of Yang-Lee zeros (15), the free energy is a continuous function of  $F$  when passing through the point  $F = F^*$  as it should be; this can be seen by inserting  $\cos(\theta/2) = \sqrt{1 - e^{-4F^*}}$  into (8) taking in the limit  $F \rightarrow F^{*-}$  and comparing to (21) taking in the limit  $F \rightarrow F^{*+}$ . As concerns the derivative of the free energy with respect to the coupling  $F$ , it diverges for  $F \rightarrow F^{*-}$  and converges to a finite number when  $F \rightarrow F^{*+}$  which signalizes a first-order phase transition at the transient point  $F^*$ . It should be emphasized that as the set of Yang-Lee zeros (15) is dense in the limit  $N \rightarrow \infty$ , the above mathematical analysis is of limited physical interest.

The magnetization per site (7)

$$m_N = 2i \frac{\partial \varphi}{\partial \theta} \tan(\varphi N) \quad (22)$$

oscillates with increasing  $N$  and so it does not exhibit a well defined thermodynamic limit in the low-temperature region  $F > F^*$ .

### III. MAPPING ONTO A SYMMETRIC VERTEX MODEL

In this section, we consider a spin- $\frac{1}{2}$  Ising model on a general  $D$ -dimensional lattice structure with coordination number  $q = 2, 3, \dots$ . The spin Hamiltonian  $H$  is given by

$$-\beta H = F \sum_{\langle j,k \rangle} s_j s_k + i \frac{\theta}{2} \sum_j s_j, \quad (23)$$

where the first sum goes over all nearest-neighbor pairs of lattice sites and the second sum over all lattice sites. The partition function is defined by (2).

In Ising systems, microscopic spins  $s = \pm 1$  are associated with lattice sites and the nearest-neighbor spins interact along edges connecting the nearest-neighbor vertices. In two-state vertex models, microscopic states  $\sigma = \pm 1$  are attached to the edges of the lattice. For a given ‘‘global’’ configuration of edge states, every vertex sees a ‘‘local’’ configuration of edge states with the corresponding Boltzmann vertex weight. The partition function of the vertex system is defined by

$$Z = \sum_{\{\sigma\}} \prod (\text{weights}), \quad (24)$$

where the sum goes over all configurations of edge states and the product is over all vertex weights in the lattice. A special case of two-state vertex systems is a *symmetric* vertex model whose local vertex weights depend only on the number of incident edges in, say,  $(-)$  state; in other words, for a vertex, any permutation of edge states in space leaves the local vertex weight invariant.

Every system of Ising spins on a lattice can be mapped onto a symmetric two-state vertex model formulated on the same lattice structure by using mapping methods [10, 19] based on a gauge transformation [20] which represents a generalization of the duality transformation and the weak-graph expansion [21]. The mapping depends on whether the spin coupling  $F$  is ferromagnetic or antiferromagnetic.

#### A. Ising antiferromagnet

In the case of an antiferromagnetic coupling  $F < 0$  it holds that  $F = -|F|$ . The Ising model on a lattice with

the coordination number  $q$  can be represented as a vertex system when one decorates each edge by a new two-coordinated vertex and attach to line fragments two-state variables  $\sigma = \pm 1$ . To reproduce the partition function of the Ising model, one attaches to the new decoration vertices the  $2 \times 2$  interaction matrix

$$\mathbf{V} \equiv \begin{pmatrix} V_{+,+} & V_{+,-} \\ V_{-,+} & V_{-,-} \end{pmatrix} = \begin{pmatrix} e^F & e^{-F} \\ e^{-F} & e^F \end{pmatrix} \quad (25)$$

and to the vertices of the original lattice with a local configuration of adjacent edges  $\{\sigma_1, \sigma_2, \dots, \sigma_q\}$  the vertex weights

$$v(\sigma_1, \sigma_2, \dots, \sigma_q) = e^{i\frac{\theta}{2}} \delta(\sigma_1, +) \delta(\sigma_2, +) \cdots \delta(\sigma_q, +) \\ + e^{-i\frac{\theta}{2}} \delta(\sigma_1, -) \delta(\sigma_2, -) \cdots \delta(\sigma_q, -). \quad (26)$$

In this way, two admissible configurations around a vertex on the original lattice, all adjacent edges in the same either  $(+)$  or  $(-)$  state, are identified with the  $(+)$  or  $(-)$  state of the spin on that vertex. For a given edge composed of two line fragments in states  $\sigma'$  and  $\sigma''$ , the contribution to the partition function can be schematically expressed as

$$\sum_{\sigma', \sigma''} v(\dots, \sigma', \dots) V_{\sigma', \sigma''} v(\dots, \sigma'', \dots). \quad (27)$$

The interaction matrix (25) can be written as product of a matrix  $\mathbf{W}$  and its transpose  $\mathbf{W}^T$  in many ways; let us apply the following factorization

$$\mathbf{V} = \mathbf{W} \mathbf{W}^T, \quad \mathbf{W} = \begin{pmatrix} \sqrt{\cosh F} & i\sqrt{\sinh |F|} \\ \sqrt{\cosh F} & -i\sqrt{\sinh |F|} \end{pmatrix}. \quad (28)$$

The next step is to use the relation  $V_{\sigma', \sigma''} = \sum_{\sigma} W_{\sigma', \sigma} W_{\sigma'', \sigma}$  in (27) to eliminate the decoration vertices by attaching  $\mathbf{W}$  to the left endpoint and  $\mathbf{W}^T$  to the right endpoint of each edge. In this way one obtains the pure two-state vertex model on the original lattice structure defined by the vertex weights

$$w(\sigma_1, \sigma_2, \dots, \sigma_q) = \sum_{\sigma'_1, \sigma'_2, \dots, \sigma'_q = \pm} v(\sigma'_1, \sigma'_2, \dots, \sigma'_q) \\ \times W_{\sigma'_1, \sigma_1} W_{\sigma'_2, \sigma_2} \cdots W_{\sigma'_q, \sigma_q}. \quad (29)$$

Explicitly,

$$w(\sigma_1, \sigma_2, \dots, \sigma_q) = e^{i\frac{\theta}{2}} W_{+, \sigma_1} W_{+, \sigma_2} \cdots W_{+, \sigma_q} \\ + e^{-i\frac{\theta}{2}} W_{-, \sigma_1} W_{-, \sigma_2} \cdots W_{-, \sigma_q}. \quad (30)$$

These vertex weights are invariant with respect to any permutation of edge states and therefore they correspond to a symmetric vertex model. It stands to reason that the partition function of the original Ising model is identical by construction to the one of the symmetric vertex model on the same lattice structure.

Let for the resulting symmetric vertex model  $w_n$  ( $n = 0, 1, \dots, q$ ) be the vertex weight of edge configurations

with  $n$  adjacent edges in state  $(-)$  and the remaining  $q - n$  adjacent edges in state  $(+)$ . Then, according to (30), one has

$$w_n = e^{i\frac{\theta}{2}} W_{+,-}^n W_{+,+}^{q-n} + e^{-i\frac{\theta}{2}} W_{-,-}^n W_{-,+}^{q-n}. \quad (31)$$

According to the form of the  $\mathbf{W}$ -matrix (28), the elements  $W_{++} = W_{-+} = \sqrt{\cosh F}$  and  $W_{+-} = -W_{--} = i\sqrt{\sinh F}$ , so that

$$w_n = (\cosh F)^{\frac{q-n}{2}} (\sinh |F|)^{\frac{n}{2}} i^n \left[ e^{i\frac{\theta}{2}} + (-1)^n e^{-i\frac{\theta}{2}} \right]. \quad (32)$$

For even number  $n$  of adjacent edges in state  $(-)$ , it holds that  $i^n = (-1)^{\frac{n}{2}}$ ,  $(-1)^n = 1$  and the consequent sum of the exponentials in the square brackets results in  $2 \cos\left(\frac{\theta}{2}\right)$ , i.e.,

$$w_n = 2(-1)^{\frac{n}{2}} (\cosh F)^{\frac{q-n}{2}} (\sinh |F|)^{\frac{n}{2}} \cos\left(\frac{\theta}{2}\right). \quad (33)$$

For odd  $n$ , it holds that  $i^n = (-1)^{\frac{n+1}{2}}/i$ ,  $(-1)^n = -1$  and the consequent difference of the exponentials in the square brackets, divided by  $i$ , results in  $2 \sin\left(\frac{\theta}{2}\right)$ , i.e.,

$$w_n = 2(-1)^{\frac{n+1}{2}} (\cosh F)^{\frac{q-n}{2}} (\sinh |F|)^{\frac{n}{2}} \sin\left(\frac{\theta}{2}\right). \quad (34)$$

We conclude that in the vertex picture all local Boltzmann weights are real, positive or negative, as was needed.

### B. Ising ferromagnet

To construct the mapping for the ferromagnetic Ising model, one has to divide the lattice into two interwoven sublattices  $A$  and  $B$  and to change signs of spin variables  $s_j \rightarrow -s_j$  at vertices of say the  $B$ -sublattice. This transformation has no effect on the partition function which is the sum over all spin configurations. On the other hand, the spin Hamiltonian (23) is changed to

$$-\beta H = -F \sum_{\langle j,k \rangle} s_j s_k + i\frac{\theta}{2} \sum_{j \in A} s_j - i\frac{\theta}{2} \sum_{j \in B} s_j, \quad (35)$$

i.e., the ferromagnetic coupling  $F > 0$  is changed to the antiferromagnetic one  $-F < 0$  and the sign of the imaginary magnetic field alternates with the  $A$  and  $B$  sublattices. Having the antiferromagnetic coupling one can proceed as in the previous subsection. After the mapping, the vertex weights of the symmetric vertex model depend on whether the vertex is on the sublattice  $A$  or  $B$ . If the vertex lies on the  $A$ -sublattice, the vertex weights are given by

$$w_n^{(A)} = 2(-1)^{\frac{n}{2}} (\cosh F)^{\frac{q-n}{2}} (\sinh F)^{\frac{n}{2}} \cos\left(\frac{\theta}{2}\right) \quad (36)$$

for even  $n$  and

$$w_n^{(A)} = 2(-1)^{\frac{n+1}{2}} (\cosh F)^{\frac{q-n}{2}} (\sinh F)^{\frac{n}{2}} \sin\left(\frac{\theta}{2}\right) \quad (37)$$

for odd  $n$ . If the vertex lies on the  $B$ -sublattice, the vertex weights are given by

$$w_n^{(B)} = 2(-1)^{\frac{n}{2}} (\cosh F)^{\frac{q-n}{2}} (\sinh F)^{\frac{n}{2}} \cos\left(\frac{\theta}{2}\right) \quad (38)$$

for even  $n$  and

$$w_n^{(B)} = 2(-1)^{\frac{n+1}{2}} (\cosh F)^{\frac{q-n}{2}} (\sinh F)^{\frac{n}{2}} \sin\left(\frac{\theta}{2}\right) \quad (39)$$

for odd  $n$ .

## IV. NUMERICAL METHODS

We apply two distinct numerical methods to the Ising models, which originate in the density-matrix renormalization [22–24]. Namely, we use the corner transfer matrix renormalization group (CTMRG) [25–27] and the higher-order tensor renormalization group (HOTRG) [28] methods for that purpose.

1) The CTMRG method comes from the Baxter's corner-transfer-matrix approach, originally proposed for the square-lattice Ising spins [29]. CTMRG is used in this work to evaluate the von Neumann entropy

$$S = -\text{Tr}(\rho \ln \rho). \quad (40)$$

Here,  $\rho$  represents a reduced density matrix, which is used for the construction of the renormalization transformations. At  $\theta = 0$ , the Ising critical point is  $F = F_c = \frac{1}{2} \ln(1 + \sqrt{2})$  [14], in which the von Neumann entropy  $S$  logarithmically diverges with respect to number of the spins  $N$  [30, 31]

$$S \sim \frac{c}{12} \ln N, \quad F = F_c. \quad (41)$$

The parameter  $c$  is an anomaly number (also known as the central charge) determining the universality class of the statistical system. For the 2D Ising model at zero magnetic field, the anomaly number  $c = \frac{1}{2}$ . We first evaluate the  $N$ -dependence of an effective anomaly number at criticality  $F_c$ ,

$$c_{\text{eff}}(N) = 12 \frac{\partial S}{\partial \ln N}. \quad (42)$$

Finally, the asymptotic value of  $c_{\text{eff}}(N)$  yields

$$c = \lim_{N \rightarrow \infty} c_{\text{eff}}(N). \quad (43)$$

2) The HOTRG method is applied to the calculation of the free energy (for both the antiferromagnet and the ferromagnet) in standard way. In the symmetry broken

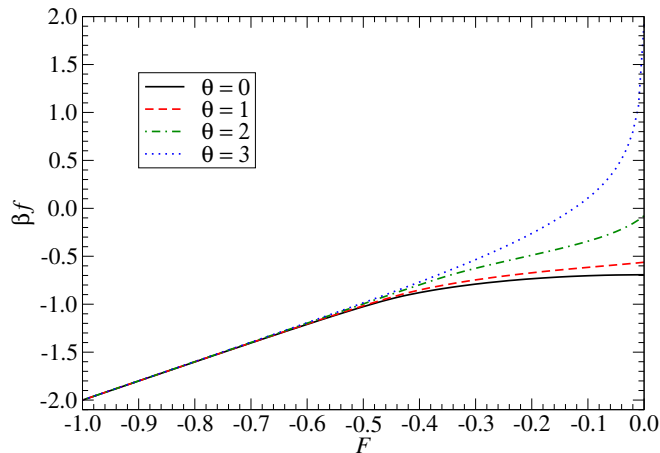


FIG. 1. The (dimensionless) free energy per spin  $\beta f$  of the 2D antiferromagnetic Ising model versus the coupling  $F \leq 0$  for four values of the (dimensionless) imaginary magnetic field  $\beta H = i\theta/2$ : zero field  $\theta = 0$  (solid curve),  $\theta = 1$  (dashed curve),  $\theta = 2$  (dash-dotted curve) and  $\theta = 3$  (dotted curve).

phase ( $F > F_c$ ) of the Ising antiferromagnet, the magnetizations per spin  $m_A$  and  $m_B$ , associated with the two sublattices  $A$  and  $B$ , respectively, differ. Hence, nonzero magnetization difference results in

$$m_{AB} = m_A - m_B \neq 0. \quad (44)$$

Since it is not straightforward how to evaluate the imaginary magnetization  $m_{AB}$  by HOTRG, we proposed an *extended* impurity tensor  $T_{AB}$  in order to distinguish the symmetry broken phase from the disordered one. It is so because there is no concise way of how to observe the  $Z_2$  broken symmetry, provided that the real (non-imaginary) character of HOTRG tensors has to be preserved. Further details of constructing the impurity-tensor are briefly described in Appendix.

## V. NUMERICAL RESULTS FOR THE 2D ANTIFERROMAGNET

Using the vertex representation of the 2D Ising antiferromagnet on the square lattice ( $q = 4$ ) derived in Sec. III A, the dependence of the (dimensionless) free energy per spin  $\beta f$  on the coupling  $F \leq 0$  is pictured in Fig. 1 for the zero magnetic field  $\theta = 0$  (solid curve) and three values of the imaginary magnetic field  $\theta = 1$  (dashed curve),  $\theta = 2$  (dash-dotted curve) and  $\theta = 3$  (dotted curve); the same notation will be used in what follows. The spins become uncoupled in the limit  $F \rightarrow 0$ , so the curves end up at the points  $\beta f = -\ln[2 \cos(\theta/2)]$ . The free energy is always an increasing function of the coupling  $F$ . In the low-temperature region, for small enough antiferromagnetic coupling  $F \lesssim -0.5$ , the curves approach close to each other. An analogous behavior is observed also in 1D.

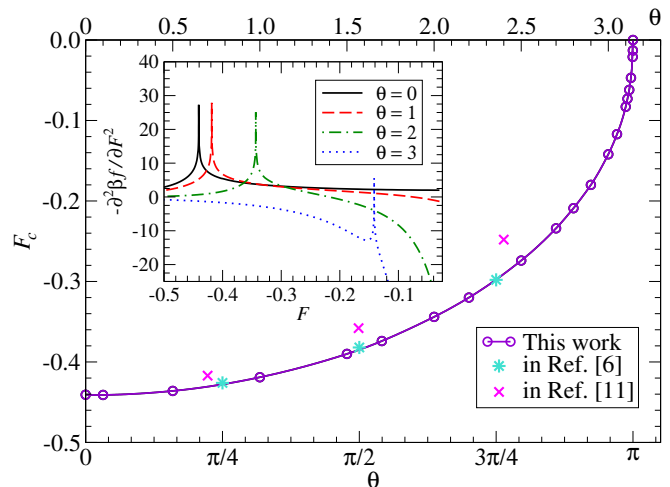


FIG. 2. Antiferromagnet: The value of the critical coupling  $F_c$  as the function of the imaginary magnetic field  $\theta \in [0, \pi]$ . The present data (open circles) are compared with the ones of Ref. [6] (stars) and Ref. [11] (crosses). The  $F$ -dependence of the second derivative of the free energy  $\beta f$  with respect to  $F$  is pictured in the inset for four values 0, 1, 2, 3 of the imaginary magnetic field  $\theta$ ; the cusp divergence of the second derivative determines the critical point  $F_c(\theta)$ .

The phenomenon which does not occur in 1D is seen in the inset of Fig. 2 where the  $F$ -dependence of the second derivative of the free energy  $\beta f$  with respect to  $F$  is represented for four values 0, 1, 2, 3 of the imaginary magnetic field  $\theta$ . For each  $\theta$ , there is a critical point  $F_c$  at which the second derivative goes to  $-\infty$ . The dependence of critical points  $F_c$  on the imaginary magnetic field  $\theta \in [0, \pi]$  is pictured in the main body of Figure 2. The present data (open circles) are compared with numerical data from other works. The data of Ref. [6] (stars), obtained by calculating complex-temperature zeros of the partition function for finite lattices of relatively small sizes, are in a good agreement with our data. The data of Ref. [11] (crosses), obtained by extrapolation of the high-temperature cumulant expansion of the free energy into the critical region, deviate much more from our data. This is caused by the fact that only the first eight cumulants were taken into account. The numerical estimate of  $F_c \approx -0.4410$  for the zero magnetic field  $\theta = 0$  is in good agreement with the exact value  $F_c = -0.44068679\dots$  obtained by Onsager [14]. The exact value  $F_c = 0$  for  $\theta = \pi$  [15] is also reproduced by our numerical calculations. Note that a similar curve of critical points occurs for the 2D Ising antiferromagnet in *real* non-zero magnetic fields [9, 10].

Figure 3 shows the dependence of the magnetization difference between the  $A$  and  $B$  sublattices, namely the real quantity  $-im_{AB}$ , on the coupling  $F$  for three values of the imaginary field  $\theta = 1, 2, 3$ ; the spontaneous magnetization for the zero magnetic field  $\theta = 0$  is presented as well. The magnetization difference is zero above the

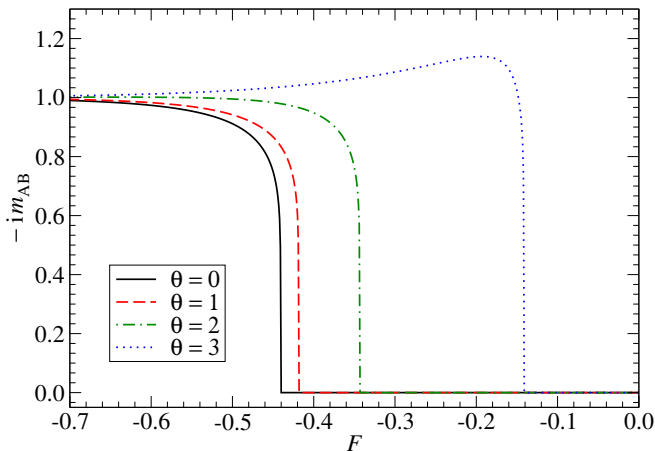


FIG. 3. Antiferromagnet: The plot of the difference between sublattice magnetizations (44)  $-im_{AB}$  versus the coupling  $F$ , for imaginary fields  $\theta = 1, 2, 3$ . The spontaneous magnetization for the zero magnetic field  $\theta = 0$  is drawn for comparison.

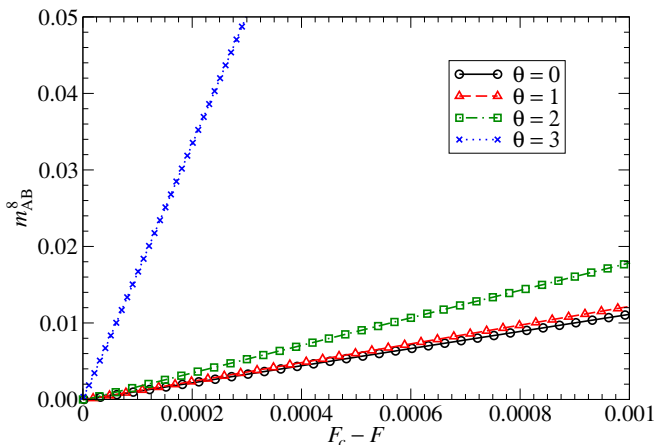


FIG. 4. Antiferromagnet: The linear dependence of the 8th power of the difference between sublattice magnetizations in the ordered phase on small deviations from the critical coupling  $F_c(\theta) - F$  for the zero magnetic field  $\theta = 0$  and the values  $\theta = 1, 2, 3$  of the imaginary field. The linear form of the plots indicates the uniformity of the critical index  $\beta = \frac{1}{8}$  along the line of critical points when changing the parameter  $\theta \in [0, \pi]$ .

critical coupling  $F_c$  and goes to 1 for asymptotically large  $F \rightarrow -\infty$ . The plot of the function  $-im_{AB}(F)$  is non-monotonous for  $\theta = 3$ , it acquires a maximum larger than 1. This confirms that also the spontaneous magnetization difference between two alternating sublattices can be larger than 1 for imaginary magnetic fields.

The dependence of  $m_{AB}^8$  on small deviations from the critical coupling  $F_c(\theta) - F$  for zero magnetic field  $\theta = 0$  and the imaginary fields  $\theta = 1, 2, 3$  is pictured in Fig. 4. The linear form of the plots indicates that the critical exponent  $\beta$  is constant along the whole curve of critical

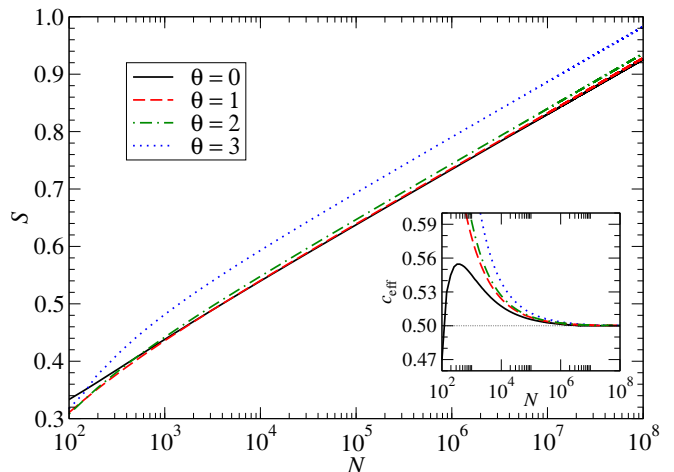


FIG. 5. Antiferromagnet: The plot of the von-Neumann entropy  $S$  versus the number of sites of the square lattice  $N$ , in the logarithmic scale. The inset shows that with increasing  $N$  the effective anomaly number  $c_{\text{eff}}(N)$  (42) tends to the Ising value  $\frac{1}{2}$ , for the zero magnetic field  $\theta = 0$  as well as the values  $\theta = 1, 2, 3$  of the imaginary magnetic field.

points  $F_c(\theta)$ , equal to its zero-field Ising value  $\frac{1}{8}$ . This behavior, which agrees with the universality hypothesis [29, 32], was observed also for the 2D Ising antiferromagnet in real non-zero magnetic fields [10].

The plot of the von-Neumann entropy  $S$  versus the number of sites  $N$  of the square lattice is pictured in the logarithmic scale in Fig. 5. It is evident that for large  $N$  the entropy grows in accordance with the expected asymptotic formula (41). The inset documents the tendency of the effective anomaly number  $c_{\text{eff}}(N)$  to the Ising value  $\frac{1}{2}$  with increasing  $N$ , for the zero field  $\theta = 0$  as well as for any value  $\theta = 1, 2, 3$  of the imaginary magnetic field. This means that the presence of the imaginary magnetic field does not change the universality class of the Ising antiferromagnet and all critical exponents remain the same as those in the zero field.

## VI. NUMERICAL RESULTS FOR THE 2D FERROMAGNET

Using the vertex representation of the 2D Ising ferromagnet on the square lattice ( $q = 4$ ) derived in Sec. III B, the dependence of the (dimensionless) free energy  $\beta f$  on the ferromagnetic coupling  $F > 0$  is pictured in Fig. 6, for zero magnetic field  $\theta = 0$  and the values  $\theta = 1, 2, 3$  of the imaginary field. The antiferromagnetic region of the couplings  $F \in [-0.1, 0]$  is included to describe in detail the neighborhood of the point  $F = 0$ . While for the zero field the free energy as the function of  $F$  decays monotonously, for the imaginary magnetic fields  $\beta f$  first grows in the region of small  $F$  up to a maximum point and then decays monotonously up to  $F \rightarrow \infty$ . The curves

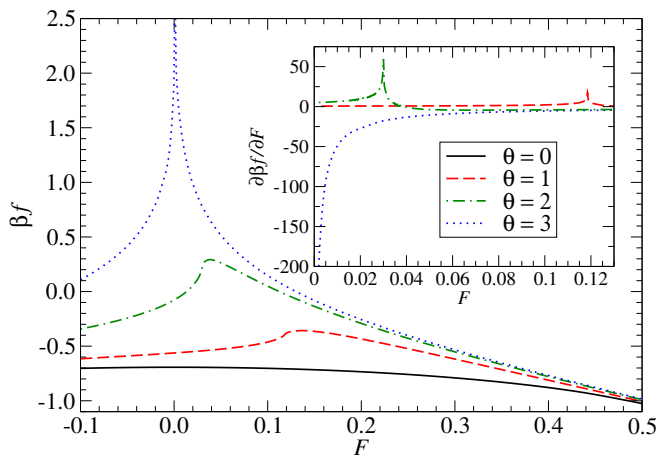


FIG. 6. Ferromagnet: The free energy  $\beta f$  as the function of the ferromagnetic coupling  $F > 0$  for zero magnetic field  $\theta = 0$  and the values  $\theta = 1, 2, 3$  of the imaginary field. The inset shows the  $F$ -dependence of the first derivative of the free energy with respect to  $F$ ; the cusp divergence of the derivative signals a first-order transition at the coupling  $F^*(\theta)$ . The free energy is well defined in the high-temperature region  $F < F^*(\theta)$ , the continuous plot of the free energy in the low-temperature region  $F > F^*(\theta)$  ignores the divergence of  $\beta f$  at a dense set of Yang-Lee zeros.

are close to each other in the low-temperature region, namely for large enough couplings  $F \gtrsim 0.5$ . The inset of Fig. 6 shows the  $F$ -dependence of the first derivative of the free energy with respect to  $F$ ; the cusp divergence of the derivative signals a first-order phase transition at the transient coupling  $F^*(\theta)$ .

To explain our numerical data for the free energy in more detail, we recall that, in analogy with the 1D version of the model, the free energy is expected to be well defined in the high-temperature region  $F < F^*(\theta)$ . In this region, being sufficiently far away from  $F^*(\theta)$  we calculate the free energy at equidistant points on the  $F$ -axis with the step  $\Delta F = 0.01$ . When the free energy starts to vary substantially, i.e. when one is close to the transient point  $F^*(\theta)$ , in order to describe correctly the neighborhood of  $F^*(\theta)$  the equidistant step is changed to the smaller one  $\Delta F = 0.0001$ . Passing through the transient point  $F^*(\theta)$ , the free energy changes smoothly once again and one returns to the previous step  $\Delta F = 0.01$ . It stands to reason that in the low-temperature region  $F > F^*(\theta)$  there exist the problematic dense set of Yang-Lee zeros of the partition function at which the free energy per site blows up to infinity. As is evident from Fig. 6, our choice of the rational equidistant points on the  $F$ -axis does not involve Yang-Lee zeros and the numerical plot of the free energy versus  $F$  looks to be continuous. This mathematical peculiarity of limited physical interest is in close analogy with the 1D version of the Ising ferromagnet and we suggest that one has to be precisely at a Yang-Lee zero to observe the divergence of the free

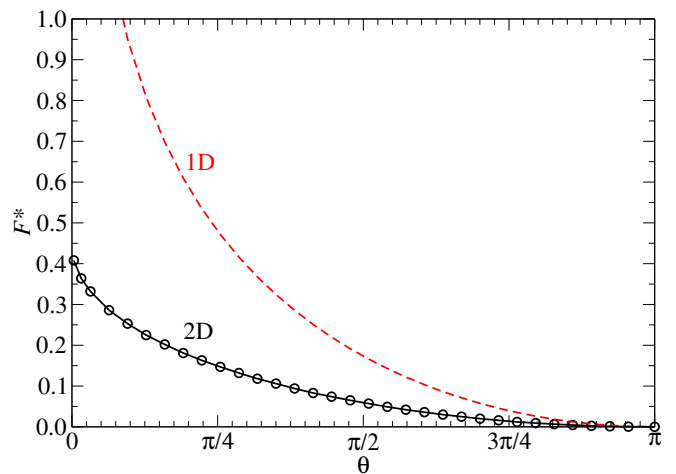


FIG. 7. Ferromagnet: The transition coupling  $F^*$  as the function of the imaginary magnetic field  $\theta$ . The analytic 1D result (10) is drawn by the dashed curve, the numerical 2D data are represented by open circles.

energy.

The dependences of the first-order transition coupling  $F^*$  on the imaginary magnetic field  $\theta$  in 1D and 2D are pictured in Fig. 7. The analytic 1D result (10) is drawn by the dashed curve. It is seen that as  $\theta \rightarrow 0$  the coupling  $F^* \rightarrow \infty$  which is in agreement with the fact that for the Ising ferromagnet in zero magnetic field there is neither first-order phase transition nor the divergence of the magnetization. The numerical 2D data for the dependence  $F^*(\theta)$  are represented in Fig. 7 by open circles. For each  $\theta$ , the value of the 2D  $F^*(\theta)$  is always smaller than the one in 1D. The limiting  $\theta \rightarrow 0^+$  value of  $F(\theta)$  is a finite number. The 2D Ising ferromagnet at the strictly zero magnetic field  $\theta = 0$  exhibits no first-order phase transition and, consequently,  $F^*(0)$  does not exist.

The divergence of the magnetization  $-im$  when the coupling constant  $F$  approaches the transition coupling  $F^*(\theta)$  (vertical dotted lines) from below (i.e., from the high-temperature region) is represented in Fig. 8. The dashed curve corresponds to the imaginary magnetic field  $\theta = 1$  and the dash-dotted curve to  $\theta = 2$ . Data for the imaginary magnetic field  $\theta = 3$  are omitted since  $F^*(3)$  is very close to zero which causes numerical instabilities in the calculation of the magnetization plot. The values of  $F^*(\theta)$  obtained in this way coincide with a high accuracy with the previous ones obtained from the divergence of the first derivative of the free energy, see Fig. 7. The high-temperature expansion of the magnetization for the Ising model on the square lattice in a magnetic field in powers of the nearest-neighbor coupling is written in Eq. (1.8.7) of monograph [29]. Inserting there imaginary field, one



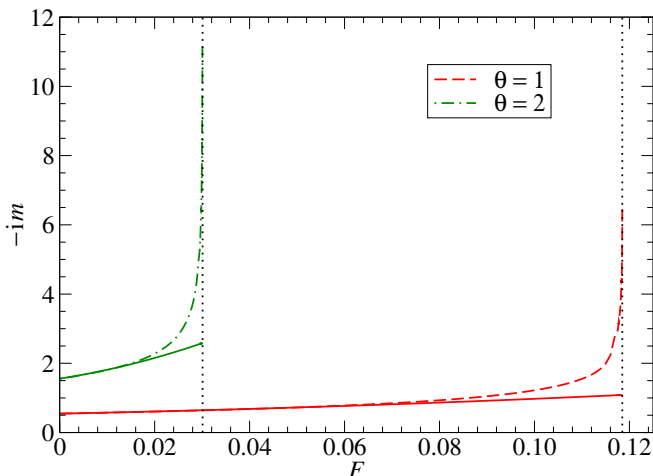


FIG. 8. Ferromagnet: The divergence of the magnetization  $-im$  for the 2D Ising ferromagnet in an imaginary field as the coupling constant  $F$  approaches the transition coupling  $F^*(\theta)$  (vertical dotted lines) from below; the imaginary magnetic field  $\theta = 1$  (dashed curve) and  $\theta = 2$  (dash-dotted curve). The dependences of  $-im$  versus  $F$  yielded by the asymptotic  $F \rightarrow 0$  formula (45) are depicted by the solid lines.

obtains

$$-im = \tan\left(\frac{\theta}{2}\right) + \frac{4 \tan\left(\frac{\theta}{2}\right)}{\cos^2\left(\frac{\theta}{2}\right)} F + \frac{4 \tan\left(\frac{\theta}{2}\right)}{\cos^2\left(\frac{\theta}{2}\right)} \left[ 3 + 7 \frac{\sin^2\left(\frac{\theta}{2}\right)}{\cos^2\left(\frac{\theta}{2}\right)} \right] F^2 + \mathcal{O}(F^3). \quad (45)$$

The dependences of  $-im$  on  $F$  yielded by this asymptotic relation are depicted for the imaginary fields  $\theta = 1, 2$  in Fig. 8 by the solid lines for comparison. When  $F > F^*(\theta)$ , the thermodynamic limit of the magnetization changes chaotically with the system size (not shown in the figure) and so it is ill-defined like in 1D.

## VII. CONCLUSION

The Ising model in a pure imaginary magnetic field exhibits a severe sign problem. The Boltzmann weight of a configuration of spins on the lattice is a complex number which prevents from application of standard methods in equilibrium statistical mechanics. We avoid this problem by mapping the considered Ising model on the square lattice onto the symmetric vertex model (with the permutation symmetry of local vertex weights) formulated on the same lattice structure in Sec. III. The mapping depends on whether the Ising nearest-neighbor couplings are antiferromagnetic (Sec. III A) or ferromagnetic (Sec. III B). The local vertex weights of the symmetric vertex model are real (positive or negative) numbers. This fact permits us to apply the accurate numerical CTMRG and HOTRG methods based on the renormalization of the density ma-

trix. Another potential application of the mapping onto the symmetric vertex model with real vertex weights is to search for the Yang-Lee zeros of the Ising partition function on finite lattices, e.g., with periodic boundary conditions.

The numerical results for the 2D antiferromagnet in an imaginary magnetic field are presented in Sec. V. The curve of critical points separating the ordered antiferromagnetic and the disordered paramagnetic phases of the model in Fig. 2 is estimated with the numerical precision of order 0.2% which substantially overcomes the accuracy of other methods [6, 11]. Data for the magnetization difference between two interwoven sublattices as the function of the coupling  $F$  are pictured in Fig. 3. It is seen that for the sufficiently high imaginary field  $\theta = 3$  the spontaneous difference between the sublattice magnetizations turns out to be larger than one in an interval of the couplings  $F$ . As concerns the critical properties, there is numerical evidence that the critical exponent  $\beta$  (Fig. 4) and the anomaly number  $c$  (Fig. 5) do not depend on the strength of the imaginary magnetic field and are equal to the zero-field Ising values  $\beta = \frac{1}{8}$  and  $c = \frac{1}{2}$ .

The phase properties of the 2D ferromagnetic Ising model in an imaginary magnetic field, studied in Sec. VI, are qualitatively similar to those of its 1D version (Sec. II B). In particular, there is a first-order transition coupling  $F^*(\theta)$  at which both the first derivative of the free energy with respect to the coupling and the magnetization diverge when approaching to  $F^*(\theta)$  from the high-temperature side,  $F \rightarrow F^{*-}$ . The free energy and the magnetization per site are well defined in the high-temperature region  $F < F^*(\theta)$ . In the low-temperature region  $F > F^*(\theta)$ , the free energy blows up at couplings which correspond to the Yang-Lee zeros of the partition function. As is evident from Fig. 6, our choice of equidistant rational points on the  $F$ -axis does not involve Yang-Lee zeros and the numerical plot of the free energy versus  $F$  looks to be smooth. This mathematical curiosity of limited physical interest was explained on the exactly solvable 1D ferromagnet in Sec. II B based on plausible arguments. The magnetization depends chaotically on the system size for  $F > F^*(\theta)$  and therefore it is ill-defined for both 1D and 2D. The only fundamental difference between 1D and 2D comes from Fig. 7: while the zero-field  $\theta \rightarrow 0$  limit of  $F^*(\theta)$  goes continuously to the expected value  $\infty$  in 1D, it approaches to a finite value in 2D and does not exist at the strictly zero field  $\theta = 0$ .

## ACKNOWLEDGMENTS

The support received from the Grants VEGA Nos. 2/0123/19 and 2/0092/21, Joint Research Project SAS-MOST 108-2112-M-002-020-MY3 and Project APVV-20-0150 is acknowledged.

## APPENDIX

Let the standard impurity tensor  $T_m$  be given by the product of the vertex weights, see (30). The standard impurity tensor is used to evaluate the magnetization according to  $m = \text{Tr}(T_m)$ . For a spatially homogeneous system on the square lattice with the coordination number  $q = 4$ , the standard impurity tensor reads

$$T_m(\sigma_1, \sigma_2, \sigma_3, \sigma_4) = \sum_{\sigma'_1, \sigma'_2, \sigma'_3, \sigma'_4 = \pm} v_m(\sigma'_1, \sigma'_2, \sigma'_3, \sigma'_4) \times W_{\sigma'_1, \sigma_1} W_{\sigma'_2, \sigma_2} W_{\sigma'_3, \sigma_3} W_{\sigma'_4, \sigma_4} \quad (46)$$

with the vertex tensor  $v_m$  being

$$v_m(\sigma_1, \sigma_2, \sigma_3, \sigma_4) = e^{i\frac{\theta}{2}} \prod_{j=1}^4 \delta(\sigma_j, +) - e^{-i\frac{\theta}{2}} \prod_{j=1}^4 \delta(\sigma_j, -). \quad (47)$$

For the inhomogeneous system, however, the sublattices magnetizations  $m_A$  and  $m_B$  are not identical in the symmetry broken state anymore. Then, the impurity tensor has to be redefined to describe the nonzero difference of the magnetization  $m_{AB} = m_A - m_B = \max(T_{AB})$ . We, therefore, consider the maximal absolute value of the extended impurity tensor  $T_{AB}$  (rather than its trace). The construction of  $T_{AB}$  was carried out by means of additional four extended impurity tensors  $T_1^A$ ,  $T_2^A$ ,  $T_1^B$ , and  $T_2^B$ , such that

$$T_{AB} = T_1^A + T_2^A - T_1^B - T_2^B. \quad (48)$$

These extended impurity tensors have doubled ranks, because the degrees of freedom on the edges of the tensors

are squared, while the coordination number still remains unchanged ( $q = 4$ ). The four tensors satisfy the relations

$$T_1^A(\{\sigma_1 \bar{\sigma}_1\}, \{\sigma_2 \bar{\sigma}_2\}, \{\sigma_3 \bar{\sigma}_3\}, \{\sigma_4 \bar{\sigma}_4\}) = \prod_{\sigma'_1, \sigma'_2, \sigma'_3, \sigma'_4} T_m(\bar{\sigma}_1, \sigma_2, \sigma'_1, \sigma'_4) w(\sigma'_1, \bar{\sigma}_2, \bar{\sigma}_3, \sigma'_2) \times w(\sigma'_3, \sigma'_2, \sigma_3, \bar{\sigma}_4) w(\sigma_1, \sigma'_4, \sigma'_3, \sigma_4), \quad (49)$$

$$T_2^A(\{\sigma_1 \bar{\sigma}_1\}, \{\sigma_2 \bar{\sigma}_2\}, \{\sigma_3 \bar{\sigma}_3\}, \{\sigma_4 \bar{\sigma}_4\}) = \prod_{\sigma'_1, \sigma'_2, \sigma'_3, \sigma'_4} w(\bar{\sigma}_1, \sigma_2, \sigma'_1, \sigma'_4) w(\sigma'_1, \bar{\sigma}_2, \bar{\sigma}_3, \sigma'_2) \times w(\sigma'_3, \sigma'_2, \sigma_3, \bar{\sigma}_4) T_m(\sigma_1, \sigma'_4, \sigma'_3, \sigma_4), \quad (50)$$

$$T_1^B(\{\sigma_1 \bar{\sigma}_1\}, \{\sigma_2 \bar{\sigma}_2\}, \{\sigma_3 \bar{\sigma}_3\}, \{\sigma_4 \bar{\sigma}_4\}) = \prod_{\sigma'_1, \sigma'_2, \sigma'_3, \sigma'_4} w(\bar{\sigma}_1, \sigma_2, \sigma'_1, \sigma'_4) T_m(\sigma'_1, \bar{\sigma}_2, \bar{\sigma}_3, \sigma'_2) \times w(\sigma'_3, \sigma'_2, \sigma_3, \bar{\sigma}_4) w(\sigma_1, \sigma'_4, \sigma'_3, \sigma_4), \quad (51)$$

$$T_2^B(\{\sigma_1 \bar{\sigma}_1\}, \{\sigma_2 \bar{\sigma}_2\}, \{\sigma_3 \bar{\sigma}_3\}, \{\sigma_4 \bar{\sigma}_4\}) = \prod_{\sigma'_1, \sigma'_2, \sigma'_3, \sigma'_4} w(\bar{\sigma}_1, \sigma_2, \sigma'_1, \sigma'_4) w(\sigma'_1, \bar{\sigma}_2, \bar{\sigma}_3, \sigma'_2) \times T_m(\sigma'_3, \sigma'_2, \sigma_3, \bar{\sigma}_4) w(\sigma_1, \sigma'_4, \sigma'_3, \sigma_4). \quad (52)$$

Within the HOTRG method, the impurity tensors iteratively expand into the doubled ranks and renormalize back to their original ranks. They represent linear combinations of all possible positions of the magnetic tensor (with the appropriate sign) divided by number of the combinations taken.

- 
- [1] K. Uzelac, R. Jullien, and P. Pfeuty, One-dimensional transverse-field Ising model in a complex longitudinal field from a real-space renormalization-group method at  $T = 0$ , Phys. Rev. B **22**, 436 (1980).
- [2] G. von Gehlen, Critical and off-critical analysis of the Ising quantum chain in an imaginary field, J. Phys. A: Math. Gen. **24**, 5371 (1991).
- [3] T. Deguchi and P. K. Ghosh, The exactly solvable quasi-Hermitian transverse Ising model, J. Phys. A: Math. Theor. **42**, 475208 (2009).
- [4] V. Matveev and R. Shrock, Complex-temperature properties of the 2D Ising model with  $\beta H = \pm i\pi/2$ , J. Phys. A: Math. Gen. **28**, 4859 (1995).
- [5] V. Matveev and R. Shrock, Complex-temperature properties of the two-dimensional Ising model for nonzero magnetic field, Phys. Rev. E **53**, 254 (1996).
- [6] V. Matveev and R. Shrock, On properties of the Ising model for complex energy/temperature and magnetic field, J. Phys. A: Math. Theor. **41**, 135002 (2008).
- [7] S.-Y. Kim, Yang-Lee zeros of the antiferromagnetic Ising model, Phys. Rev. Lett. **93**, 130604 (2004).
- [8] E. Müller-Hartmann and J. Zittartz, Interface free energy and transition temperature of the square-lattice Ising antiferromagnet at finite magnetic field, Z. Phys. B **27**, 261 (1977).
- [9] F. Y. Wu, X. N. Wu, and H. W. J. Blöte, Critical frontier of the antiferromagnetic Ising model in a magnetic field: The honeycomb lattice, Phys. Rev. Lett. **62**, 2773 (1989).
- [10] M. Kolesík and L. Šamaj, New variational series expansions for lattice models, J. Phys. I France **3**, 93 (1993).
- [11] V. Azcoiti, G. Di Carlo, E. Follana, and E. Royo-Amondarain, Antiferromagnetic Ising model in an imaginary field, Phys. Rev. E **96**, 032114 (2017).
- [12] V. Azcoiti, E. Follana, and A. Vaquero, Progress in numerical simulations of systems with a  $\theta$ -vacuum like term: The two and three-dimensional Ising model within an imaginary magnetic field, Nucl. Phys. B **851** [FS], 420 (2011).
- [13] V. Azcoiti, V. Laliena, and A. Galante, QCD with a  $\theta$ -vacuum term: A complex system with a simple complex action, in: Proceedings of the International Workshop on Non-Perturbative methods and Lattice QCD, Guangzhou, China, p.161 (2000).
- [14] L. Onsager, Crystal statistics. I. A two-dimensional model with an order disorder transition, Phys. Rev. **65**, 117 (1944).

- [15] T. D. Lee and C. N. Yang, Statistical theory of equations of state and phase transitions. II. Lattice gas and Ising model, *Phys. Rev.* **87**, 410 (1952).
- [16] V. Azcoiti and A. Galante, Parity and CT realization in QCD, *Phys. Rev. Lett.* **83**, 1518 (1999).
- [17] I. S. Gradshteyn and I. M. Ryzhik, *Table of Integrals, Series, and Products*, 6th ed. (Academic Press, London, 2000).
- [18] M. Abramowitz and I. A. Stegun, *Handbook of Mathematical Functions with Formulas, Graphs, and Mathematical Tables*, 9th ed. (Dover, New York, 1972).
- [19] L. Šamaj and M. Kolesík, Mapping of the symmetric vertex model onto the Ising model for an arbitrary lattice coordination, *Physica A* **182**, 455 (1992).
- [20] F. J. Wegner, A transformation including the weak-graph theorem and the duality transformation, *Physica* **68**, 570 (1973).
- [21] J. F. Nagle, Weak-graph method for obtaining formal series expansions for lattice statistical problems, *J. Math. Phys.* **9**, 1007 (1968).
- [22] S. R. White, Density matrix formulation for quantum renormalization groups, *Phys. Rev. Lett.* **69**, 2863 (1992).
- [23] S. R. White, Density-matrix algorithms for quantum renormalization groups, *Phys. Rev. B* **48**, 10345 (1993).
- [24] U. Schollwöck, The density-matrix renormalization group, *Rev. Mod. Phys.* **77**, 259 (2005).
- [25] T. Nishino and K. Okunishi, Corner transfer matrix renormalization group method, *J. Phys. Soc. Jpn.* **65**, 891 (1996).
- [26] T. Nishino and K. Okunishi, Corner transfer matrix algorithm for classical renormalization group, *J. Phys. Soc. Jpn.* **66**, 3040 (1997).
- [27] K. Ueda, R. Otani, Y. Nishio, A. Gendiar, and T. Nishino, Critical point of a symmetric vertex model, *J. Phys. Soc. Jpn.* **74**, 1871 (2005).
- [28] Z. Y. Xie, J. Chen, M. P. Qin, J. W. Zhu, L. P. Yang, and T. Xiang, Coarse-graining renormalization by higher-order singular value decomposition, *Phys. Rev. B* **86**, 045139 (2012).
- [29] R. J. Baxter, *Exactly Solved Models in Statistical Mechanics*, 3rd ed. (Dover Publications, London, 2007).
- [30] P. Calabrese and J. Cardy, Entanglement entropy and quantum field theory, *J. Stat. Mech.* P06002 (2004).
- [31] E. Ercolessi, S. Evangelisti, and F. Ravanini, Exact entanglement entropy of the XYZ model and its sine-Gordon limit, *Phys. Lett. A* **374**, 2101 (2010).
- [32] L. Šamaj and Z. Bajnok, *Introduction to the Statistical Physics of Integrable Many-body Systems*, (Cambridge Univ. Press, Cambridge, 2013).